Supporting Information

Stepwise oxidation strategy for the synthesis of amorphous V_2O_5@V_2CT_x nanohybrid cathodes toward high-performance aqueous Zn-ion batteries

Weiwei, Wang,[a] Ruiting Hu,[a] Chi Zhang,[a] Yu Tao,[a] Ling Ran,[a] Yani Li,[a] Yao, Ouyang,[d] and Jun, Yan *[a b c]

[a] *College of Chemistry and Chemical Engineering, Central South University, Changsha 410083, Hunan, P. R. China.*

[b] *Hunan Provincial Key Laboratory of Efficient and Clean Utilization of Manganese Resources, Changsha 410083, Hunan, P. R. China.*

[c] *Hunan Provincial Key Laboratory of Chemical Power Sources, Changsha 410083, Hunan, P. R. China.*

[d] *Chang Jun High School of Changsha, Changsha 410083, Hunan, P. R. China.*

First-Principle DFT Calculations

All computations are carried out in the framework of density generalized function theory, using a projector augmented plane-wave approach, implemented in the Vienna Vienna *ab-initio* simulation package [1]. The generalized gradient approximation proposed by Perdew, Burke, and Ernzerhof was chosen as the exchange-correlation potential [2]. The plane wave cut-off energy was set to 450 eV. The energy criterion was set as 10^{-5} eV in iterative solution of the Kohn-Sham equation. The Brillouin zone integration was performed using a 3×3×3 *k*-mesh for VO_2 2×2×2 supercell, 5×5×3 *k*-mesh for $Zn_3OH_2V_2O_7$ and $Zn_3OH_2V_2O_7{\cdot}2H_2O$, and 3×3×3 *k*-mesh for the amorphous V_2O_5 2×2×2 supercell, which is obtained through the AIMD method we have used the NVT ensemble with a timestep of 1 fs for 3000 fs at 1250 K. All the structures were relaxed until the residual forces on the atoms have declined to less than 0.02 eV/Å. Zn ion diffusion barriers and transition states in VO_2 2×2×2 supercell, $Zn_3OH_2V_2O_7$, $Zn_3OH_2V_2O_7{\cdot}2H_2O$ and V_2O_5 2×2×2 was determined using the climbing image nudged elastic band (CINEB) method [3, 4]. All calculations of this work were performed through the MedeA VASP 6.

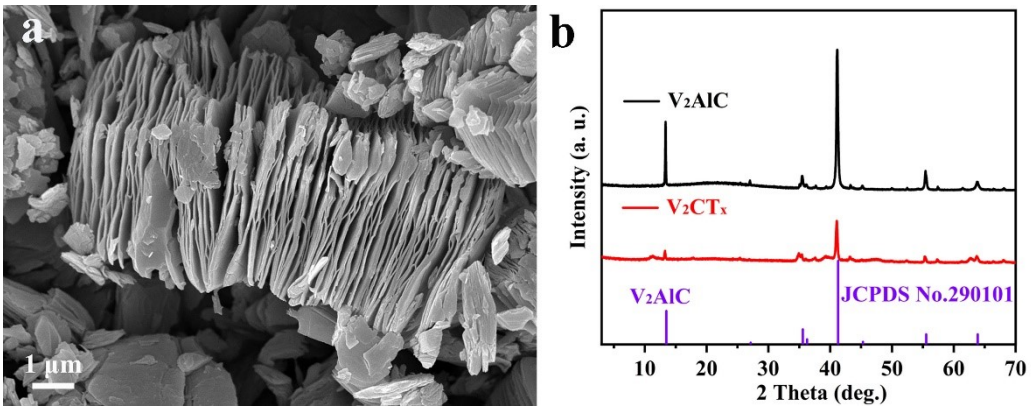

Figure S1. (a) SEM image and (b) XRD pattern of V_2CT_x.

The weak diffraction peaks located at around 11.2° appeared after chemical etching, which is assigned to the (002) plane of V_2CT_X MXene. Importantly, the position of this peak tends to shift slightly depending on the amount of enclosed water intercalated between the MXene layers, which in turn may change with different synthesis conditions. The small peaks of 13.5° and 41.5° around 2θ indicate the presence of a small amount of unreacted crystalline V_2AlC MAX phase (JCPDS No. 290101). This small amount of unreacted MAX phase appears in almost all MXenes synthesized by HF etching, and due to its more ordered structure compared to the produced MXene, its XRD peak is relatively sharp. In addition, SEM shows the formation of the typical accordion-like multilayered MXene structure of V_2CT_x.

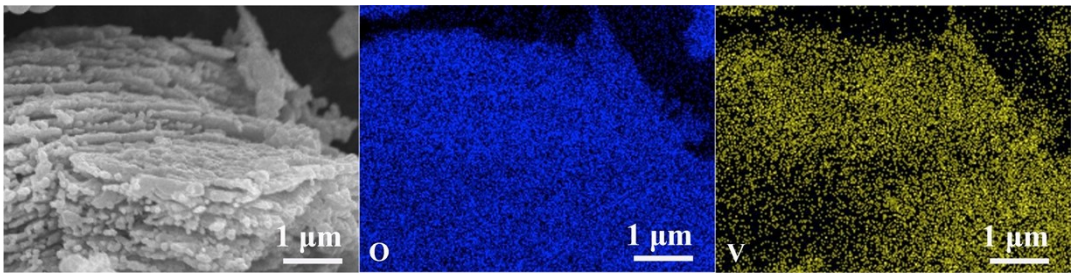

Figure S2. SEM elemental mapping images of the VO2(M)@V2CTx-600 materials

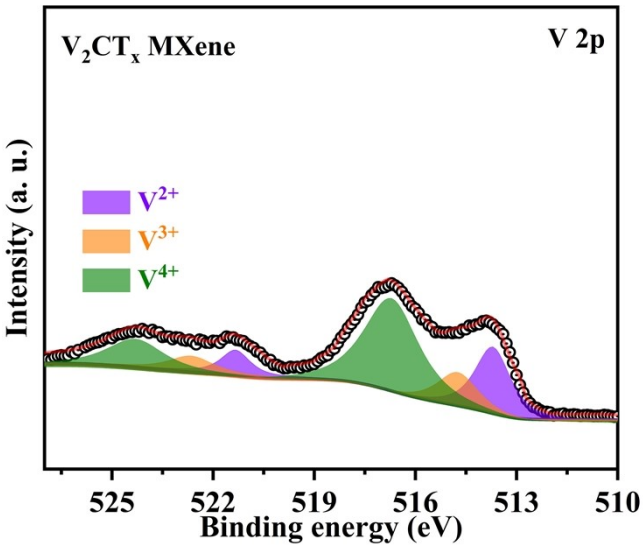

Figure S3. V 2p spectrum of V_2CT_x MXene.

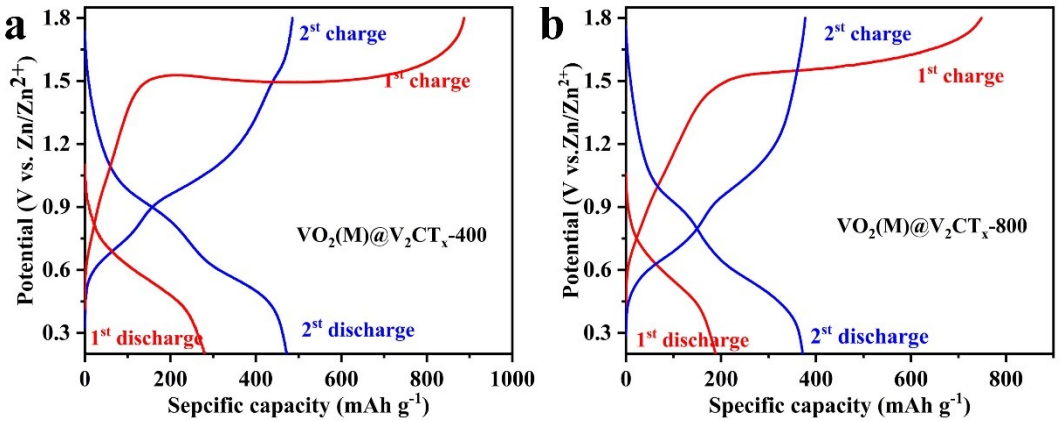

Figure S4. GCD curves of (a) the VO_2(M)@V_2CT_x-400 and (b) VO_2(M)@V_2CT_x-800 electrodes in the 1 cycle and 2nd cycle.

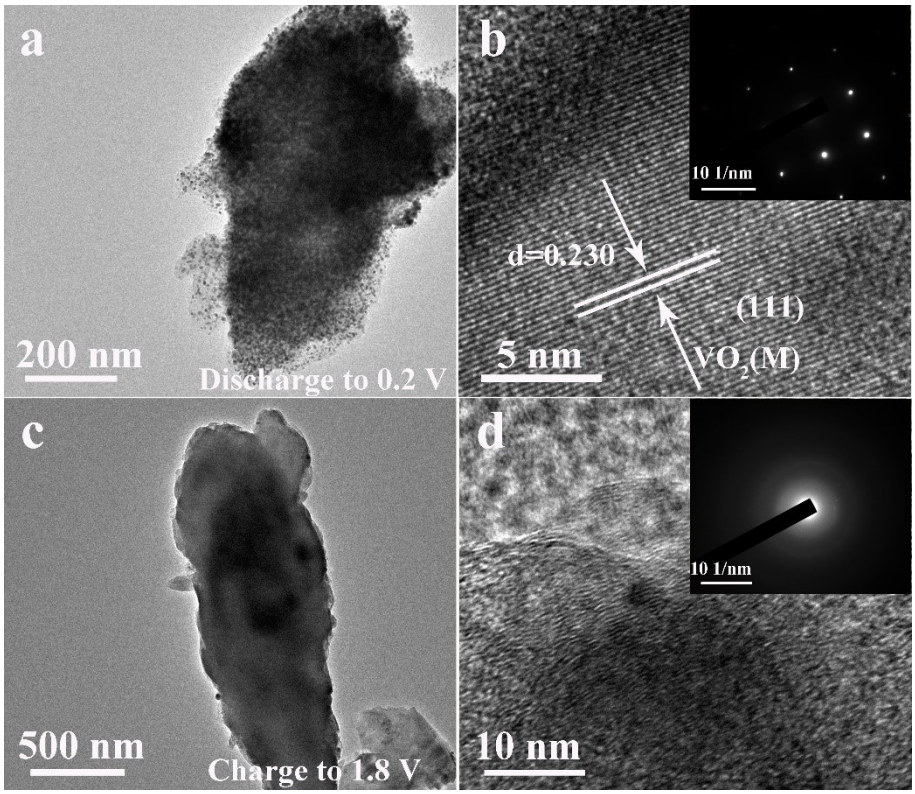

Figure S5. TEM analysis of VO_2(M)@V_2CT_x-600 cathode at selected voltage.

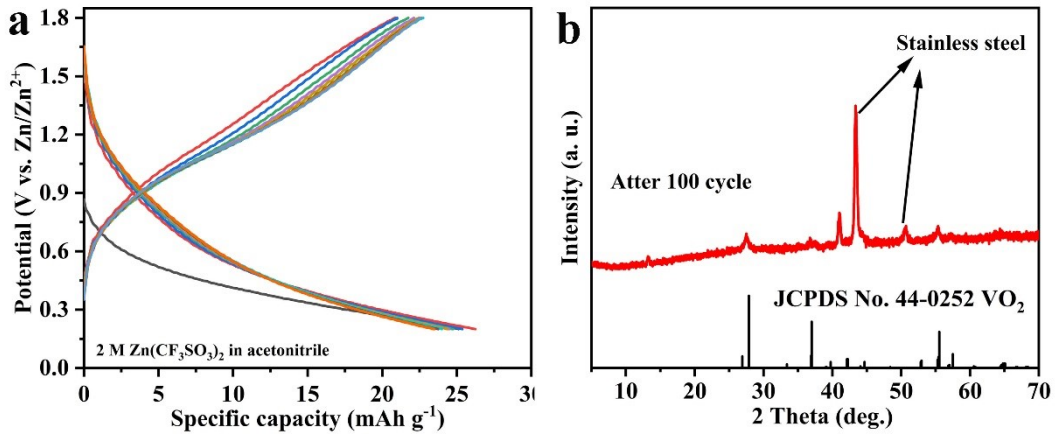

Figure S6. (a) GCD curves and (b) XRD pattern of the VO_2(M)@V_2CT_x-600 electrode in 2 M $Zn(CF_3SO_3)_2$ in acetonitrile.

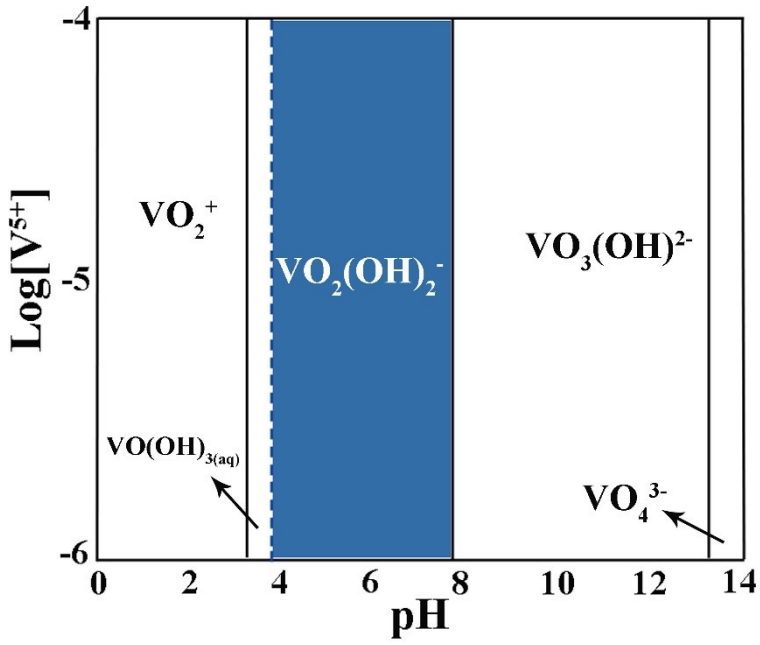

Figure S7. Predominant V^{5+} species in aqueous solutions at 25 °C as a function of vanadium concentration ($[V^{5+}]$) and pH.[5]

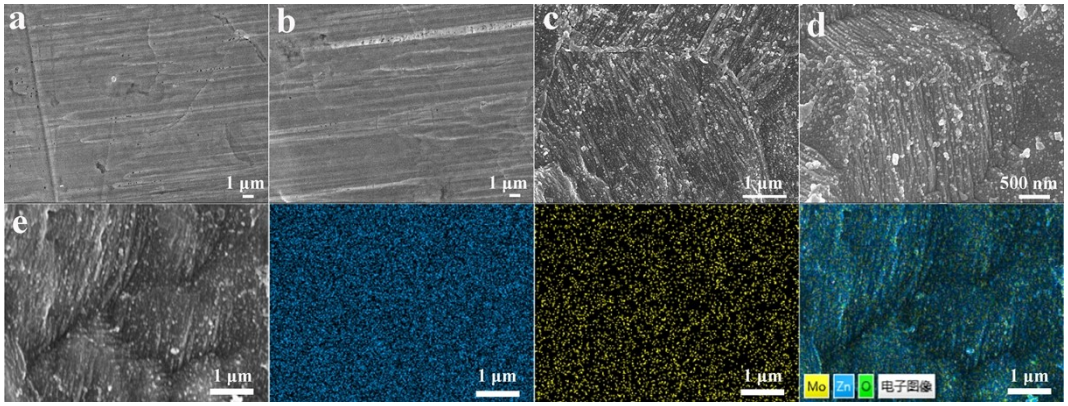

Figure S8. (a, b) SEM images of the bare Zn. (c, d) SEM images and corresponding element mapping (e) of Zn@$ZnMoO_4$.

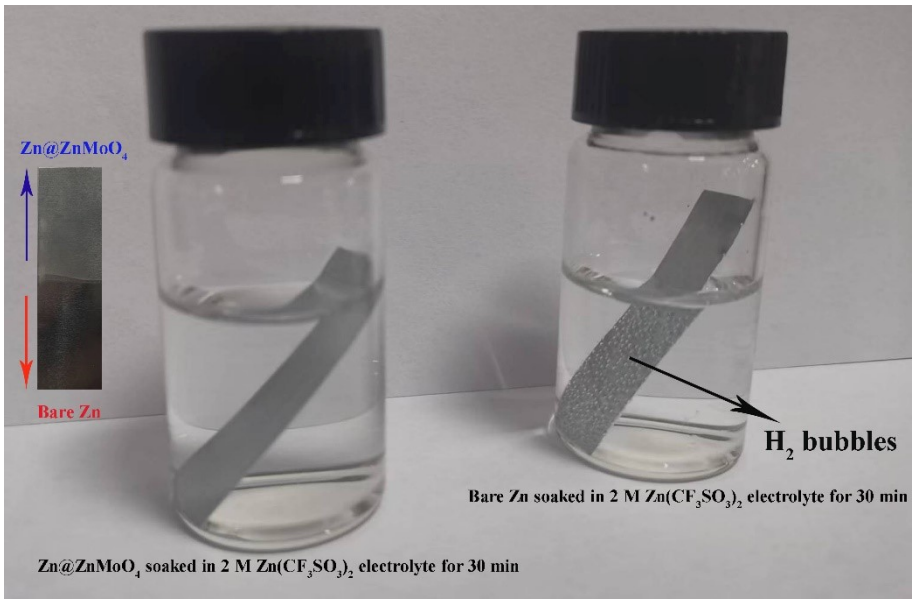

Figure S9. Digital photographs of $Zn@ZnMoO_4$ and bare Zn immersed in 2M $Zn(CF_3SO_3)_2$ electrolyte.

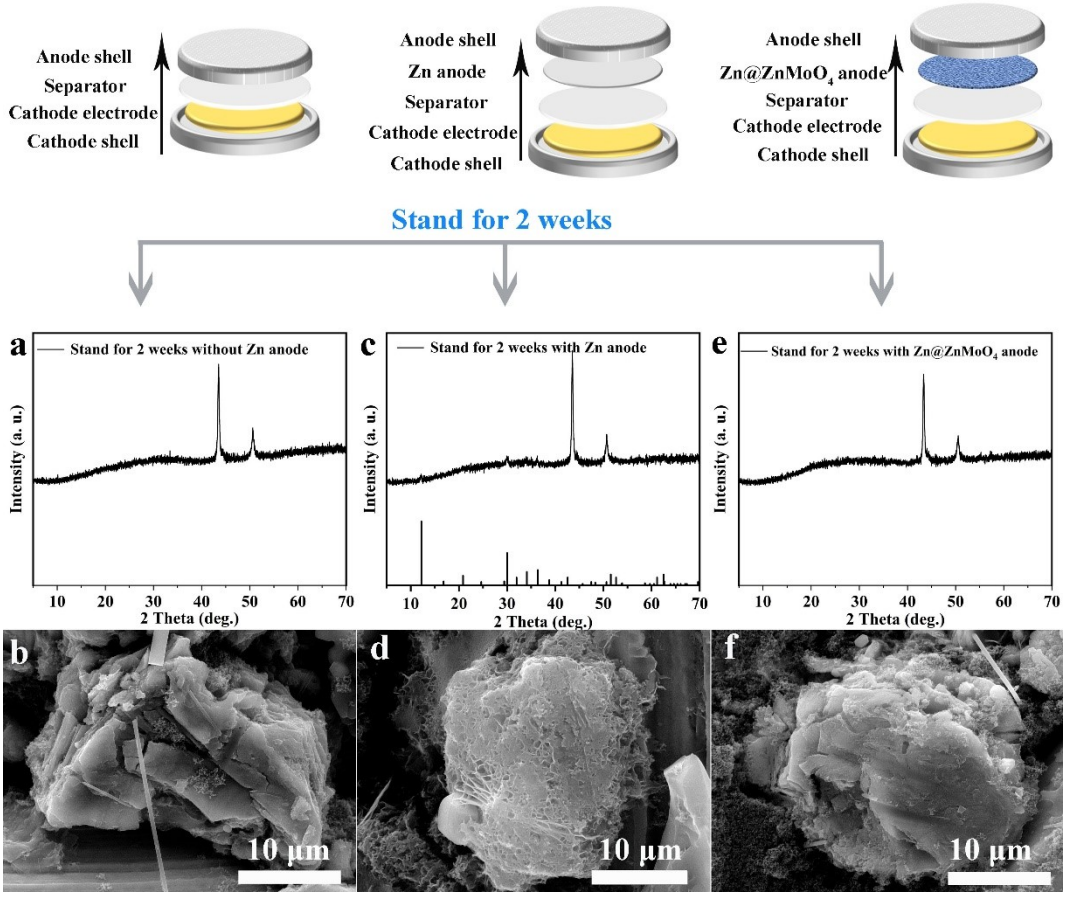

Figure S10. Sketches of the cell models of a-V_2O_5@V_2CT_x//without Zn anode, amorphous V_2O_5@V_2CT_x//with Zn anode and the amorphous V_2O_5@ V_2CT_x// with Zn@$ZnMoO_4$ anode batteries and their corresponding XRD pattern and SEM image after 2 weeks of standing.

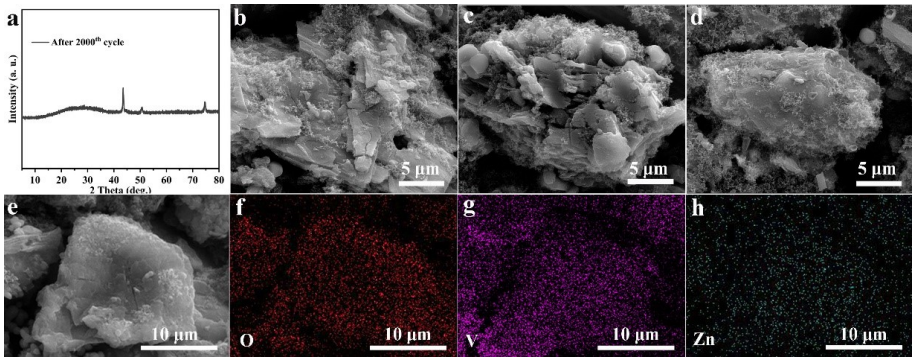

Figure S11. (a) XRD pattern, (b-d) SEM images, and (e-h) SEM element mapping of the amorphous $V_2O_5@V_2CT_x$ cathode after 2000^{th} cycle.

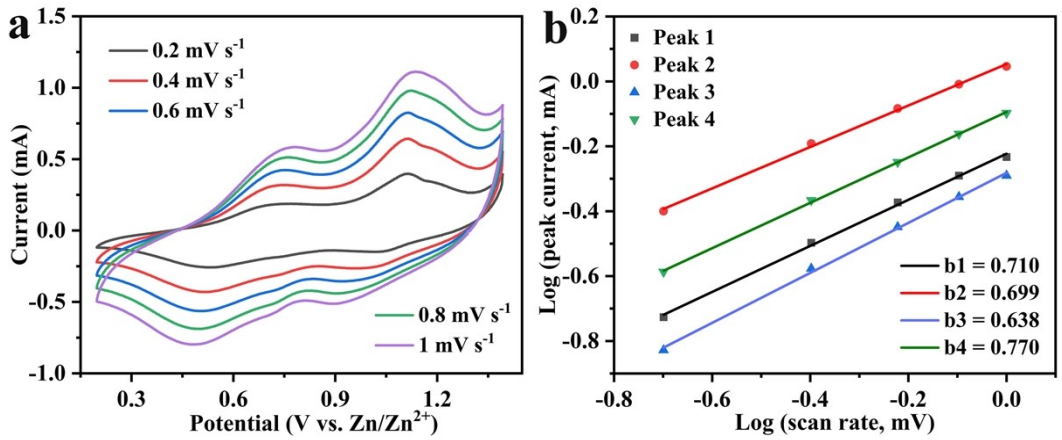

Figure S12. (a) CV curves, and (b) relationship between the logarithm of peak current and logarithm of scan rate of the VO_2(M)@V_2CT_x-600.

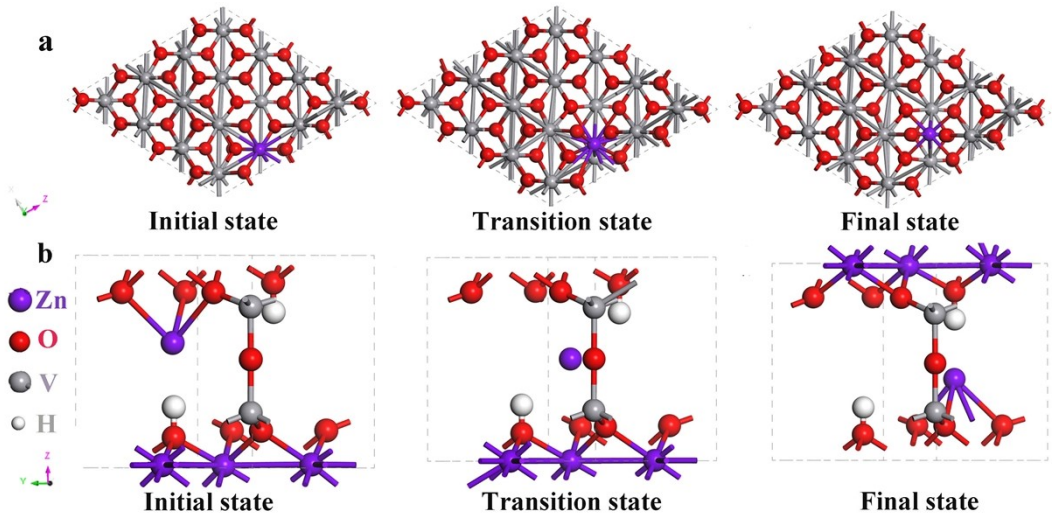

Figure S13. (a, b) initial state, transition state and final state of immigration path of Zn in VO_2(M) and $Zn_3OH_2V_2O_7$, respectively.

In the ZVO crystal structure, Zn atoms occupy the octahedral sites in a close-packed layer of O atoms; thus, Zn atoms in the layers are difficult to move. Although the [ZnO_6] layers are connected by pyrovanadatem groups and forms an open framework, it exhibits much higher Zn^{2+} diffusion barriers than those of than VO_2(M) and amorphous V_2O_5.

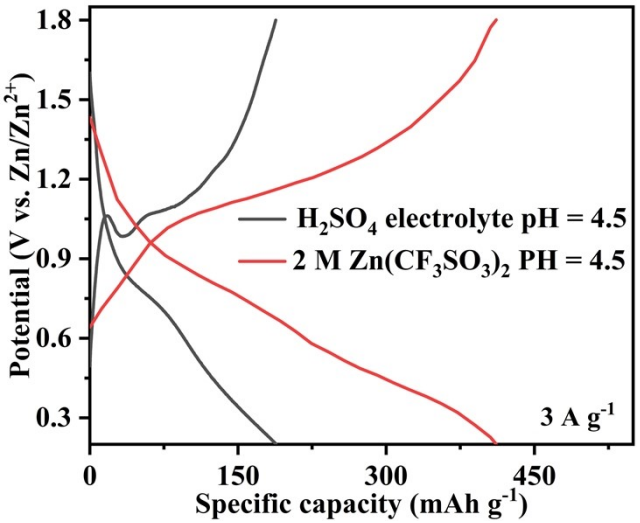

Figure S14. GCD curves of the amorphous V_2O_5@V_2CT_x cathode at 3 A g^{-1} in H2SO4 and Zn(CF3SO3)2 electrolyte.

Table S1. Electrochemical performance comparisons of the amorphous V_2O_5@V_2CT_x with the recently reported Zn-ion battery cathodes.

Cathode	Potential window	Specific capacity	Rate capacity	Cycling performance	Ref.
Amorphous V_2O_5@V_2CT_x	0.2-1.8 V	651 mA h g^{-1} at 0.1 A g^{-1}	302 mA h g^{-1} at 20 A g^{-1}	405 mA h g^{-1} at 2 A g^{-1} after 2000 cycles. (93% retention)	**This work**
Amorphous V_2O_5/Graphene	0.2-1.8 V	489 mA h g^{-1} at 0.1 A g^{-1}	237 mA h g^{-1} at 20 A g^{-1}	240 mA h g^{-1} at 30 A g^{-1} after 3000 cycles. (87% retention)	Adv. Energy Mater. 2020, 2000081
N-doped KMn_8O_{16} with abundant oxygen vacancy	0.8-1.8 V	298 mA h g^{-1}. at 0.1 A g^{-1}	106 mA h g^{-1} at 10 A g^{-1}	262 mA h g^{-1} at 1 A g^{-1} after 2500 cycles. (91% retention)	Adv. Sci. 2022, 9, 2106067
CuMn-PBA	0.45-1.8 V	108 mA h g^{-1}. at 0.1 A g^{-1}	52 mA h g^{-1} at 2 A g^{-1}	104 mA h g^{-1} at 1 A g^{-1} after 2000 cycles. (96.8% retention)	Angew. Chem. Int. Ed. 2022, 61, e202212031
CNT-CaMO	1-1.8 V	366 mA h g^{-1}. at 0.1 A g^{-1}	104 mA h g^{-1} at 2 A g^{-1}	no obvious capacity fading during 6000 cycles at 3 A g^{-1}.	Dalton Trans., 2022, 51, 9477–9485
d-VOH@CT	0.2-1.6 V	386 mA h g^{-1}. at 0.2 A g^{-1}	168 mA h g^{-1} at 10 A g^{-1}	194 mA h g^{-1} at 5 A g^{-1} after 2000 cycles. (89% retention)	J. Mater. Chem. A, 2022, 10, 13428–13438

Amorphous V_2O_5@$Ti_3C_2T_x$	0.2-1.8 V	544 mA h g^{-1} at 0.5 A g^{-1}	144 mA h g^{-1} at 30 A g^{-1}	135 mA h g^{-1} at 30 A g^{-1} after 1000 cycles.	J. Power Sources, 2022, 544, 231883
Mn^{2+}-intercalated $V_{10}O_{24}.nH_2O$	0.2-1.6 V	403 mA h g^{-1} at 0.5 A g^{-1}	235.5 mA h g^{-1} at 22 A g^{-1}	287.6 mA h g^{-1} at 10 A g^{-1} after 25000 cycles. (92.9% retention)	Energy Stor. Materials, 2022, 45 568-577
Activated V_2CT_x	0.2-1.8 V	386 mA h g^{-1} at 1 A g^{-1}	358 mA h g^{-1} at 30 A g^{-1}	283.7 mA h g^{-1} at 30 A g^{-1} after 2000 cycles. (79.2% retention)	Adv. Funct. Mater. 2021, 31, 2008033
VSe_2@V_2CT_x	0.1-1.6 V	302 mA h g^{-1} at 0.1 A g^{-1}	132 mA h g-1 at 2 A g^{-1}	158 mA h g^{-1} at 2 A g^{-1} after 600 cycles. (93.1% retention)	ACS Nano 2022, 16, 2711−2720
VS_2/MXene	0.2-1.2 V	213.4 mA h g^{-1} at 0.2 A g^{-1}	208.7 mA h g^{-1} at 5 A g^{-1}	195 mA h g^{-1} at 5 A g^{-1} after 2400 cycles. (93.4% retention)	J. Power Sources, 2022, 545, 231944

References

1 G. Kresse, D. Joubert, *Phy. Revi. B* 1999, **59**, 1758-1775.

2 J.P. Perdew, K. Burke, M. Ernzerhof, *Phy. Rev. Lett*. 1996, **77**, 3865-3868.

3 G. Henkelman, B. P. Uberuaga; H. Jónsson, *J. Chem. Phys*. 2000, **113**, 9901-9904.

4 G. Mills, H. Jónsson, G.K. Schenter, *Surf. Sci*. 1995, **324**, 305-337.

5 Y. Kim, Y. Park, M. Kim, J. Lee, K.J. Kim, J.W. Choi, *Nat. Commun*. 2022, **13**, 2371.